To be published as a Chapter in "Nonlinear Infrared Generation," Y. R. Shen, ed., Springer-Verlag, Berlin

LBL-5117
c. 1

NONLINEAR INFRARED GENERATION

Y. R. Shen

May 1976

Prepared for the U. S. Energy Research and Development Administration under Contract W-7405-ENG-48

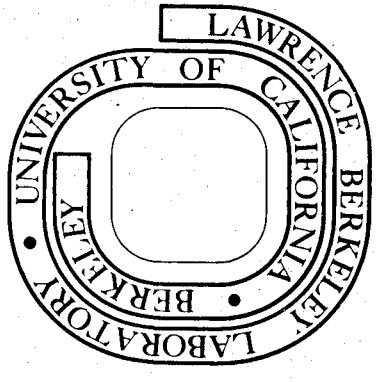

LBL-5117
c. 1

DISCLAIMER

Chapter in book of same name.
Topics Series of Applied Physics
(Springer-Verlag, Berlin)

LBL-5117

UNIVERSITY OF CALIFORNIA

Lawrence Berkeley Laboratory
Berkeley, California

AEC Contract No. W-7405-eng-48

NONLINEAR INFRARED GENERATION

Y. R. Shen

Physics Department
University of California
Berkeley, California

and

Materials and Molecular Research Division
Lawrence Berkeley Laboratory
University of California
Berkeley, California

"This work was done with support from the U. S. Energy Research and Development Administration. Any conclusions or opinions expressed in this report represent solely those of the author and not necessarily those of the Lawrence Berkeley Laboratory nor of the U. S. Energy Research and Development Administration."

LBL-5117

NONLINEAR INFRARED GENERATION

Y. R. Shen
Physics Department
University of California
Berkeley, California

and

Materials and Molecular Research Division
Lawrence Berkeley Laboratory
University of California
Berkeley, California

This book is devoted to coherent infrared generation by nonlinear optical means, particularly tunable infrared generation in the medium and far infrared range. From the scientific point of view, the need of novel infrared sources is quite obvious. Being an important field of science, infrared spectroscopy has always been lagging behind optical spectroscopy in the visible. The reasons are two fold: a) infrared detectors are not as sensitive, and b) infrared sources are not as intense. Traditionally, blackbody radiation has been the only practical infrared source. Yet dominated by the Planck distribution, it has rather weak radiative power in the medium and far infrared region. A 1-cm^2 5000°K blackbody radiates a total power of about 1000W over the 4π solid angle, but its far infrared content in the spectral range of 50 ± 1 cm^{-1} is only 3×10^{-6} W/cm^2-sterad. Weak source intensity coupled with low detector sensitivity has been the major impedance in the development of infrared science in general. Recently, infrared lasers became available. Their intensities are of course more than sufficient for ordinary spectroscopic use, yet their discrete frequencies with essentially zero tunability have left much to be desired. With the help of lasers, however, it has become possible to generate coherent tunable infrared radiation over a wide range via nonlinear processes. These include difference-frequency mixing, parametric oscillation, stimulated Raman and polariton scattering, optically pumped laser emission, and others. Coherent infrared output at an intensity level far exceeding that of any available blackbody source has already been achieved with either CW or pulsed mode of operation. The high peak intensity of the pulsed output now opens up new areas of infrared

spectroscopy, namely, transient coherent spectroscopy and nonlinear optical spectroscopy. One can expect that when these sources become readily available, the field of infrared sciences will definitely undergo a revolutionary change.

1.1 Historical Remarks.

Infrared generation by nonlinear means is actually not limited to lasers as the pump sources. For many years, electron beam tubes, such as klystron, magnetron, and carcinotron, have been used as submillimeter and far-infrared sources up to 25 cm^{-1}. Nonlinear frequency multiplication can then be used to obtain even higher frequencies. Unfortunately, the intensities of these devices drop off very rapidly with increasing frequency. With the advent of high-intensity lasers, nonlinear wave mixing can now be easily realized over a broad spectrum of electromagnetic radiation. In 1961, Franken et al. [1.1] first reported the detection of second-harmonic generation in a quartz crystal. Shortly after, Bass et al. [1.2] made the first sum-frequency mixing experiment with two different lasers. Smith and Braslau [1.3] first observed the difference-frequency generation and then Bass et al. [1.4] demonstrated the optical rectification effect. Immediately after the first second-harmonic generation experiment, the importance of phase (or momentum) matching for improvement of conversion efficiency was recognized by Giordmaine [1.5] and Maker et al. [1.6]. Other factors important for efficient nonlinear mixing such as focusing [1.7,8] and double refraction [1.9] were also studied. Many other nonlinear optical effects were discovered in the early years. Among them, parametric oscillation was first

demonstrated by Giordmaine and Miller [1.10] and stimulated Raman scattering by Woodbury and Ng [1.11].

In nonlinear infrared generation, Zernike and Bermann [1.12] first reported detection of far-infrared output from mixing of a large number of modes of a Nd:glass laser pulse in a quartz crystal. Later, Zernike [1.13] also observed far-infrared generation by mixing of two CO_2 laser frequencies in InSb. Subsequently, Yajima and Inoue [1.14] and Faries et al. [1.15] used two simultaneously Q-switched ruby lasers with different frequencies as the pump sources in optical mixing to generate far-infrared radiation. The Berkeley group [1.15] emphasized the continuous tuning aspect and studied the spectral content of the output. The Bell Lab group [1.16-20] also reported a number of difference-frequency mixing experiments in semiconductors with CO_2 lasers. They studied various phase-matching schemes in far-infrared generations. Meanwhile, parametric oscillators have been developed to cover an extended frequency range from the visible to the near infrared [1.21]. Stimulated electronic Raman scattering in metal vapor was observed by Sorokin et al. [1.22] and by Rokni and Yastiv [1.23]. Stimulated spin-flip Raman lasers tunable in the mid-infrared region were invented by Patel and Shaw [1.24]. Optically pumped far infrared molecular lasers were developed by Chang and Bridges [1.25]. Tunable far infrared output from stimulated polariton scattering was generated by Yarborough et al. [1.26]. Tunable infrared generation by difference-frequency mixing in $LiNbO_3$ was achieved by Dewey and Hocker using dye lasers [1.27].

More recently, Nguyen and Bridges [1.28] demonstrated the possibility of using a tunable spin-flip transition to resonantly enhance the far-infrared output in optical mixing. Matsumoto and Yajima [1.29] and Yang et al.

[1.30] succeeded in mixing two dye laser beams in nonlinear crystals to generate tunable far infrared radiation over a wide range. Sorokin et al. [1.31] showed that tunable infrared radiation can also be generated in vapor via third-order four-wave mixing. Lax, Aggarwal, and coworkers [1.32,33] studied extensively far infrared generation by difference-frequency mixing of two CO_2 laser beams in semiconductors. They emphasized the importance of discrete but fine tunability of the output. They, as well as Yang et al. [1.30],demonstrated the improved efficiency of far-infrared generation by optical mixing with noncollinear phase matching. Using the multiple total-reflection scheme [1.34], Aggarwal et al. [1.33] were able to improve the conversion efficiency even further and observe for the first time a detectable CW far-infrared output from difference-frequency mixing. Recently, Bridge et al. [1.35] also obtained tunable CW far-infrared output by mixing of a spin-flip Raman laser beam with a CO_2 laser beam in Te. Thompson and Coleman [1.36] succeeded in using a GaAs far-infrared waveguide as the nonlinear medium for far-infrared generation. Aside from optical mixing, stimulated Raman scattering in atomic vapor [1.37] and in molecular gas [1.38] with a tunable dye laser as the pump source, has also been used to generate tunable infrared radiation. Optically pumped high-pressure molecular gas lasers which could be tuned over limited ranges have been demonstrated [1.39]. Using a parametric oscillator for optical mixing, Byer and coworkers [1.40] are presently developing a system whose output can be continuously tuned all the way from near uv to infrared around 20μm.

There exist some other schemes of nonlinear infrared generation.

Auston et al. [1.41] studied far infrared generation by optical mixing resulting from optical excitation of absorbing defects or impurities. Yang et al. [1.42] and also Yajima and Takeuchi [1.43] reported the generation of far infrared short pulses through optical rectification of picosecond optical pulses. Byer and Herbst [1.44] succeeded in generating tunable infrared radiation by four-wave Raman mixing process in molecular gases. Granatstein et al. [1.45] observed intense tunable submillimeter radiation from relativistic electrons moving in a spatially varying magnetic field.

The field of nonlinear infrared generation is relatively new. While there exist numerous review articles on special topics such as parametric oscillators (see Chapter 3), stimulated spin-flip Raman lasers [1.46, 47] and optically pumped gas lasers (see Chapter 6), the only one on far infrared generation is by Shen [1.48].

1.2 Infrared Generation by Optical Mixing

Optical mixing is by far the most frequently employed method for nonlinear infrared generation. The basic theory for optical mixing is well-known [1.49]. The field $\vec{E}(\omega)$ generated by optical mixing is governed by

$$\nabla \cdot [\overleftrightarrow{\epsilon}(\omega) \cdot \vec{E}(\omega) + 4\pi \vec{P}^{NL}(\omega)] = 0$$

$$[\nabla \times (\nabla \times) - \omega^2 \epsilon(\omega)/c^2]\vec{E}(\omega) = (4\pi\omega^2/c^2)\vec{P}^{NL}(\omega) \qquad (1.1)$$

where $\overleftrightarrow{\epsilon}$ is the linear dielectric constant of the medium and $\vec{P}^{NL}(\omega)$ is the nonlinear polarization induced by beating of the pump fields. Consider

for example difference-frequency mixing in a crystal. We have in the second-order electric-dipole approximation

$$\vec{P}^{NL}(\omega) = \overleftrightarrow{\chi}^{(2)}(\omega = \omega_1 - \omega_2) : \vec{E}(\omega_1)\vec{E}^*(\omega_2) \tag{1.2}$$

where $\overleftrightarrow{\chi}^{(2)}$ is the second-order nonlinear susceptibility and $\vec{E}(\omega_1)$ and $\vec{E}(\omega_2)$ are the pump fields.

The solution of Eqs. (1.1) and (1.2) in the diffractionless limit is fairly simple and is to be discussed in some detail in Chapters 2 and 3. For difference-frequency generation of infinite plane waves in a semi-infinite medium along $\hat{z}$, we find the well-known result

$$|\vec{E}(\omega, z = \ell)|^2 = |\frac{2\pi\omega^2}{c^2 k_z} P^{NL}(\omega)|^2 [\frac{\sin(\Delta k\ell/2)}{(\Delta k\ell/2)}]^2 \ell^2 \tag{1.3}$$

where $\Delta k = (\vec{k}_1 - \vec{k}_2 - \vec{k}) \cdot \hat{z}$ is the phase mismatch in the $\hat{z}$ direction. It shows that the efficiency of difference-frequency generation is a maximum at $\Delta k = 0$. In practice, one should also consider the effects of finite beam cross-sections, focusing, absorption, double refraction, etc. These will be discussed in Chapters 2 and 3 by adopting the formalism developed in the literature for sum-frequency and second-harmonic generation.

However, if the difference-frequency is small, then there are actually important differences between sum-and difference-frequency generation. First, when the wavelength becomes comparable to the beam dimensions, diffraction is no longer negligible. Second, for a crystal slab of thickness ℓ, the approximate phase matching condition $\Delta k\ell \ll 1$ can be

satisfied for difference-frequency wavevectors extending over a broad cone angle. Third, the refractive index of a condensed matter at the infrared is often large (~5), and therefore, the boundary effects on far-infrared difference-frequency generation can be very important. This is manifested by the fact that part of the generated radiation may suffer total reflections in the medium and never get out of the medium. Finally, the collection angle of the detector may even be smaller than the cone angle of the emitted radiation. These effects are of course more appreciable for smaller difference frequencies.

We can use a simple model to take into account these long-wavelength effects approximately. Physically, the nonlinear polarization $\vec{P}^{NL}(\omega)$ is simply a set of oscillating dipoles in the medium so that Eq. (1.1) essentially describes radiation from a dipole antenna array. The general solution of such a problem with appropriate boundary conditions is difficult, but in special cases, approximate solutions can be obtained. For example, assume there is a thin slab of nonlinear medium and the normally incident pump beams induce a $\vec{P}^{NL}(\omega)$ which can be approximated by

$$\vec{P}^{NL}(\vec{r},\omega) = \hat{x}P^{NL}\exp(ik_s z - i\omega t) \quad \text{for } (x^2 + y^2) \leq a^2$$
$$= 0 \quad \text{for } (x^2 + y^2) > a^2$$

where P^{NL} is independent of $\vec{r}$. If we neglect the boundary effects of the slab, then the usual dipole radiation theory gives us immediately the far-field solution of Eq. (1.1)

$$\vec{E}(\vec{r},\omega) = (\omega/c)^2 \int_V d^3r' (1 - \hat{r}\hat{r}) \cdot \vec{P}^{NL}(\vec{r}',\omega) e^{ik|\vec{r} - \vec{r}'|}/|\vec{r} - \vec{r}'|. \qquad (1.4)$$

By integrating the intensity over the area of a circular detector sitting on the $\hat{z}$-axis, we find the difference-frequency power collected by the detector to be [1.15]

$$W = \frac{\omega^4 \varepsilon^{\frac{1}{2}}(\omega)}{c^3} |P^{NL}(\omega)|^2 \ell^2 (\pi a^2)^2 \int_0^{\theta_m} d(\sin\theta) \sin\theta \left(\frac{\sin\alpha}{\alpha}\right)^2 \left(\frac{2J_1(\beta)}{\beta}\right)^2 \qquad (1.5)$$

where ℓ is the thickness of the slab, θ is the angle between $\hat{r}$ and $\hat{z}$, θ_m is the maximum collection angle of the detector, $\alpha = k\ell(1 - \cos\theta + \Delta k/k)/2$, $\Delta k = k_s - k$, and $\beta = ka \sin\theta$. The Bessel function term $[2J_1(\beta)/\beta]^2$ is a description of diffraction from a circular aperture, while $(\sin\alpha/\alpha)^2$ takes into account the effect of phase mismatch. In the diffractionless limit $ka \ll 1$, the term $[2J_1(\beta)/\beta]^2$ is significant only when $\theta < 1/ka$, and the integral asymptotically reduces to $(2/k^2a^2)\sin^2(\Delta k\ell/2)/(\Delta k\ell/2)^2$. Then, Eq. (1.5) reduces to the same form as the one obtained from Eq. (1.3) in the plane-wave approximation.

We can of course use a more realistic spatial distribution for $\vec{P}^{NL}(\vec{r},\omega)$, e.g., a Gaussian profile as induced by Gaussian pumped beams [1.50]. The integration in Eq. (1.4) may be more complicated, but can always be done numerically. The difficulty of the above approach is, however, in the boundary effects. Because of the large refractive indices at long wavelengths, reflection and refraction of the difference-frequency waves at the boundaries can be very important. As a crude approximation for the thin slab case, we can use an average Fabry-Perot transmission

factor

$$F = T/\left|1 - Re^{i2k\ell}\right|^2 \tag{1.6}$$

to take into account the boundary effects, where T and R are the average transmission and reflection coefficients respectively. The power collected by the detector then becomes WF. This approximation is good when the collection angle θ_m is sufficiently small. The above equations should provide a good order-of-magnitude estimate of the difference-frequency output power.

More rigorously, to take focusing, diffraction, double refraction, boundary effects, etc. all properly into account, we must use the method of Fourier analysis [1.50,51]. We first decompose the fields and the non-linear polarization into spatial Fourier components and then solve the wave equation for each Fourier component of the difference-frequency field with the proper boundary conditions. The formalism is quite similar to the one used by Bjorkholm [1.7] and Kleinman et al. [1.8] for second-harmonic generation, although it is somewhat more complicated in the long-wavelength limit. Preliminary calculations [1.50] indicate that the results obtained from Eqs. (1.4-6) are in fact a good approximation if the double refraction effect can be neglected. The frequency spectrum and the angular distribution of the difference-frequency output and the effects of focusing and double refraction on the output have also been calculated. [1.50]

The experimental status of difference-frequency generation in crystals is reviewed and summarized in Chapter 2 for output in the far-infrared region

and in Chapter 3 for output in the mid- and near-infrared region. Roughly speaking, tunable output in the range between 400 cm^{-1} and 10,000 cm^{-1} has been obtained by using either a dye laser or a parametric oscillator as the tunable pump source. Tunable output in the range between 1 cm^{-1} and 200 cm^{-1} has been obtained with ruby lasers, dye lasers, CO_2 lasers, or spin-flip Raman lasers (see Chapter 4) as the pump sources. Report on difference-frequency generation between 200 cm^{-1} and 400 cm^{-1} has, however, been rare. As shown in Eqs. (1.3) and (1.5), the difference-frequency output is proportional to ω^2 in the diffractionless limit and to ω^4 in the limit where diffraction dominates. Therefore, if the pump beam intensities and the nonlinear susceptibility remain unchanged, the efficiency of difference-frequency generation should drop appreciably as the output wavelength increases. The result is that for mid- and far-infrared generation, the power conversion efficiency is usually much less than 1%.

Nonlinear infrared generation can also be achieved with four-wave mixing in a medium with inversion symmetry [1.31,44]. In this case, three pump beams beat against one another to produce a third-order nonlinear polarization $\vec{P}^{NL}(\omega)$ at the infrared frequency. The calculation of the output is then exactly the same as the one described earlier. Normally, as a third-order term, the nonlinear polarization is very small. However, if the frequencies are close to sharp resonances, $\vec{P}^{NL}(\omega)$ can be greatly enhanced through resonant enhancement. This happens for example in gas media. Tunable infrared generation by four-wave optical mixing in atomic vapor is reviewed in Chapter 5 and the same process in hydrogen gas is discussed in Chapter 3. In experiments, long gas cells are often used to increase the interaction

length and hence improve the conversion efficiency. However, the improvement drops off quickly with decrease of output frequency as diffraction becomes more important. No far-infrared generation in a gas medium has yet been reported presumably because of the poor conversion efficiency.

1.3 Infrared Parametric Oscillators.

The subject of parametric oscillators as coherent tunable infrared sources is reviewed in Chapter 3. Physically, parametric amplification can be considered as the inverse process of sum-frequency generation ($\omega_1 + \omega_2 = \omega_3$). Energy in the pump field at ω_3 is transferred to the signal and idler fields at ω_1 and ω_2. The amplification is maximum or the oscillation threshold is minimum when the colinear phase matching condition $k_1 + k_2 = k_3$ is approximately satisfied. This phase matching condition together with the cavity condition of the parametric oscillator then selects the particular set of frequencies ω_1 and ω_2 appearing at the output. External perturbation such as temperature, crystal orientation, and dc electric field can change the wavevectors and vary the phase matching condition, and therefore can be used as a means to tune the output frequencies. The theory of parametric oscillators is given in detail in Chapter 3.

Parametric amplification was first observed by Wang and Racette [1.52] in 1965. Subsequently, parametric oscillation was observed by Giordmaine and Miller [1.10]. While work in the early days was mainly in constructing a coherent tunable source in the visible and near-infrared, the more recent activity in the field is to extend the operating range of parametric oscillators farther into the infrared. At present, with a pulsed Nd: YAG laser as the pump source, parametric oscillation has been observed down to 10.4 μm in CdSe [1.53] and from

1.22μm to 8.5μm in proustite [1.54]. In most cases, pulsed Nd: YAG lasers were used to pump parametric oscillators because of their good mode quality and high peak intensity. The present state of art on parametric oscillators is more thoroughly described in Chapter 3.

If the parametric amplification in a nonlinear crystal is sufficiently high, then the tunable output resulting from noise amplification in one traversal through the crystal can be very strong. This is known as parametric superflourescence (see Chapter 3). Clearly, for such a process to occur, a pulsed laser with a very high peak intensity is usually required to pump the nonlinear crystal. Recently, with a Nd: glass mode-locked laser as the pump source, parametric superfluorescence has been used to generate intense tunable picosecond pulses in the infrared [1.55].

1.4 Infrared Generation by Stimulated Raman and Polariton Scattering.

Stimulated Raman scattering (SRS) is another method now being used to construct practical devices that generate coherent tunable infrared radiation. The effect was discovered accidentally in 1962 by Woodbury and Ng [1.11]. In the subsequent years, it has contributed a great deal to the advance of nonlinear optics (see the review articles by Bloembergen [1.56], by Kaiser and Maier [1.57], and by Shen [1.58]).

The theory of stimulated Raman process involving a dispersionless final excitation can be described simply as follows [1.56,58]. As shown in Fig. 1.1, Raman scattering is a direct two-photon process. We shall consider here only the Stokes process. Following an intuitive physical argument, we can express the rate of Stokes amplification as

$$\frac{d\bar{n}_2}{dz} = \left(\frac{dW_{fi}}{d\omega_2}\rho_i - \frac{dW_{if}}{d\omega_2}\rho_f\right)\varepsilon_2^{\frac{1}{2}}/c - \alpha_2\bar{n}_2 \tag{1.7}$$

where $\bar{n}_1$ and $\bar{n}_2$ are the average densities of photons in the incoming laser and scattered Stokes modes respectively, ρ_i and ρ_f are the populations in the initial and final states respectively, and α_2 is the attenuation coefficient at ω_2. The differential transition probability W_{fi} from $|\, i >$ to $|\, f >$ can be easily derived from the second-order perturbation calculation. Physically, we expect to find $W_{fi} = (A/\rho_i)(d\sigma/d\Omega)\bar{n}_1(\bar{n}_2 + 1)$ and $W_{if} = (A/\rho_i)(d\sigma/d\Omega)(\bar{n}_1 + 1)\bar{n}_2$ where A is a proportional constant and $(d\sigma/d\Omega)$ is the differential spontaneous Raman cross-section. If $\bar{n}_1, \bar{n}_2 \gg 1$, we then have from Eq. (1.7),

$$\frac{d\bar{n}_2}{dz} = (G - \alpha_2)\bar{n}_2 \tag{1.8}$$

with $G = (A\varepsilon_1^{\frac{1}{2}}/c\rho_i)(d^2\sigma/d\omega_2 d\Omega)\bar{n}_1(\rho_i - \rho_f)$. The solution of Eq. (1.8) is $\bar{n}_2(z) = \bar{n}_2(o)\exp[(G - \alpha)z]$ assuming constant $\bar{n}_1$. This shows that if $G > \alpha$, then the Stokes intensity will grow exponentially until depletion of $\bar{n}_1$ or saturation sets in. The gain factor G is directly proportional to the spontaneous Raman cross-section and the pump laser intensity.

One can also obtain the above result from the usual semiclassical derivation [1.49,59]. The wave equation for the field E_2 at ω_2 is

$$\nabla \times (\nabla \times \vec{E}_2) - \frac{\omega_2^2}{c^2}\varepsilon_2\vec{E}_2 = \frac{4\pi\omega_2^2}{c^2}\vec{P}^{(3)}(\omega_2) \tag{1.9}$$

where the third-order nonlinear polarization $\vec{P}^{(3)}$ is given by

$$\vec{P}^{(3)}(\omega_2) = (\chi_{R2}^{(3)}|E_1|^2 + \chi_2^{(3)}|E_2|^2)E_2.$$

The solution of Eq. (1.9) is, assuming constant $|E_1|^2$,

$$|E_2|^2(z) = |E_2|^2(o) \exp [G_R - \alpha)z] \tag{1.10}$$

where $G_R = - (4\pi\omega_2^2/c^2k_2)(Im\chi_{R2}^{(3)})|E_1|^2$. From semiclassical derivation for a dispersionless excitation, we can show that $Im\chi_{R2}^{(3)} \propto (d^2\sigma/d\omega_2 d\Omega)(\rho_i - \rho_f)/\rho_i$, and also $G_R = G$, so that Eq. (1.10) is in fact consistent with the solution of Eq. (1.8).

More generally, however, SRS should be considered as the result of coupling between light and material excitational waves. [1.59,60]: The pump field E_1 at ω_1 beats with the Stokes field E_2 at ω_2 to excite a material excitational wave ψ at $\omega_3 = \omega_1 - \omega_2$; the latter in turn beats with the pump field to amplify the Stokes field. In general, for an infrared-active excitation, ψ can also interact directly with an infrared field E_3 at ω_3. Direct coupling of ψ and E_3 leads to a new class of excitations known as polaritons [1.61] ——— mixed em and material excitations. Typical polariton dispersion curves are shown in Fig. 1.2. The Raman process now excites a particular polariton on the dispersion curve as governed by energy and momentum conservation. Stimulated Raman scattering by polariton is known as stimulated polariton scattering (SPS). The output of SPS can be tuned if the excitation is varied along the polariton dispersion curve.

The wave equations for the coupled waves can be written as [1.58,62].

$$[\nabla^2 + \omega_2^2\varepsilon_2/c^2]E_2 = -(4\pi\omega_2^2/c^2)P^{NL}(\omega_2)$$
$$[\nabla^2 + \omega_3^2\varepsilon_3/c^2]E_3 = -(4\pi\omega_3^2/c^2)[P^{L}(\omega_3) + P^{NL}(\omega_3)] \qquad (1.11)$$
$$[\beta\nabla^2 + \hbar(\omega_3 - \omega_o + i\Gamma)]\psi = f^{L}(\omega) + f^{NL}(\omega)$$

where β, ω_o, and Γ denote respectively dispersion, resonant frequency, and damping of the material excitation, $P^{NL}(\omega_2) = -\partial F/\partial E_2^*$, $P^{L}(\omega_3) + P^{NL}(\omega_3) = -\partial F/\partial E_3^*$, and $f^{L}(\omega) + f^{NL}(\omega) = -\partial F/\partial[N(\rho_i - \rho_f)\psi^*]$, with $F = \{N[AE_3\psi^* + ME_1E_2^*\psi^*](\rho_i - \rho_f) + \chi^{(2)}E_1E_2^*E_3^* + \text{complex conj.}\}$ being the average coupling energy. N is the density of molecules or unit cells, and A, M, and $\chi^{(2)}$ are coupling constants. For simplicity, we have neglected, in the polarizations, terms which are independent of the excitation. We have also assumed $|E_1|^2$ to be a constant and neglected the pumping of population from the initial to the final state by SRS. In the language of magnetic resonance, pumping of population is known as longitudinal excitation, while excitation of ψ is known as transverse excitation.

Consider first the special case where E_3 vanishes because A = 0 and $\chi^{(2)} = 0$. Then, if the dispersion of ψ is negligible ($\beta = 0$), we can immediately find $P^{NL}(\omega_2) = \chi_{R2}^{(3)}|E_1|^2E_2$ with $\chi_{R2}^{(3)} = N|M|^2(\rho_i - \rho_f)/\hbar(\omega_3 - \omega_o - i\Gamma)$ which is exactly the same expression one would find for Raman susceptibility from a semiclassical derivation. Therefore, this is clearly the case of ordinary SRS.

Consider next SPS with $\beta = 0$. We can eliminate ψ in Eq. (1.11) and

reduce Eq. (1.11) to the form

$$[\nabla^2 + (\omega_2^2/c^2)(\varepsilon_2)_{eff}]E_2 = -4\pi(\omega_2^2/c^2\chi_{eff}^{(2)*}E_1E_3^*$$
$$[\nabla^2 + (\omega_3^2/c^2)(\varepsilon_3)_{eff}]E_3 = -4\pi(\omega_3^2/c^2)\chi_{eff}^{(2)}E_1E_2^* \qquad (1.12)$$

where

$$(\varepsilon_2)_{eff} = \varepsilon_2 + 4\pi\chi_{R2}^{(3)}|E_1|^2$$
$$(\varepsilon_3)_{eff} = \varepsilon_3 - N|A|^2(\rho_i - \rho_f)/\hbar(\omega_3 - \omega_o + i\Gamma) \qquad (1.13)$$
$$\chi_{eff}^{(2)} = \chi^{(2)} - NA^*M(\rho_i - \rho_f)/\hbar(\omega_3 - \omega_o + i\Gamma).$$

Note that $k_3 = (\omega_3/c)(\varepsilon_3)_{eff}$ governing the dispersion of E_3 is the dispersion relation for polaritons. Equation (1.12) is now in the form identical to those describing parametric amplification. (see Chapter 3)[1.49]. The solution is well-known and can be written as

$$E_2^* = [\mathcal{E}_{2+}^* \exp(i\Delta K_+ z) + \mathcal{E}_{2-}^* \exp(i\Delta K_- z)] \exp(-i\vec{k}_2\cdot\vec{r})$$
$$E_3 = [\mathcal{E}_{3+} \exp(i\Delta K_+ z) + \mathcal{E}_{3-} \exp(i\Delta K_- z)] \exp(i\vec{k}_3\cdot\vec{r} + i\Delta kz) \qquad (1.14)$$

where

$$k = (\omega/c)(\varepsilon'_{eff})^{\frac{1}{2}}$$

$$\Delta k = k_{1z} - k_{2z} - k_{3z} \quad , \quad k_z = \vec{k}\cdot\hat{z},$$

$$\Delta K_{\pm} = \frac{1}{2}(\gamma_2 - \gamma_3) \pm \frac{1}{2}[(\gamma_2 + \gamma_3)^2 - 4\Lambda]^{\frac{1}{2}}$$

$$\gamma_2 = (k_2/2k_{2z})(i\alpha_2 + 2k_R)$$

$$k_R = (\omega_2^2/2k_{2z}c^2)4\pi\chi^{(3)}_{R2}|E_1|^2$$

$$\gamma_3 = -\Delta k - i(k_3/2k_{3z})\alpha_3$$

$$\Lambda = (4\pi^2\omega_2^2\omega_3^2/c^2k_{2z}k_{3z})(\chi^{(2)}_{eff})^2|E_1|^2$$

$$|\mathcal{E}_3/\mathcal{E}_2|_{\pm} = (\omega_3^2k_{2z}/\omega_2^2k_{3z})^{\frac{1}{2}}|\Lambda^{\frac{1}{2}}(\Delta K_{\pm} + \gamma_3)|. \qquad (1.15)$$

Either ΔK_+ or ΔK_- has a negative imaginary part indicating an exponential gain for E_2 and E_3. The gain is maximum at $\Delta K = 0$ if the ω_o resonance is sufficiently narrow.

From what we have discussed, we realize that the output of SRS and SPS can be tuned by 1) using a tunable pump laser, 2) varying the excitation frequency ω_o with an external perturbation, or 3) in the case of SPS, varying the excited polariton frequency by adjusting the relative directions of beam propagation. All these methods have been used with success to generate tunable infrared radiation. Thus, SRS in vapor with a tunable pulsed dye laser as the pump source can produce tunable output from the visible down to ~670 cm^{-1}[1.37]. The peak output power can be as high as 60 MW [1.38]. The process is strongly enhanced when the pump laser frequency approaches a resonance. The experimental status of SRS in vapor is

briefly reviewed in Chapters 3 and 5.

For a magnetic excitation, ω_o can be easily adjusted by an external magnetic field. This is the case of spin-flip transitions in solids where $\omega_o = 2g\mu_B B$, with μ_B being the magneton and B is the applied magnetic field. While the spin g factors for most solids are small, the one for InSb is as large as 50 so that if B is varied from 0 to 100 KG, ω_o can be tuned from 0 to 250 cm^{-1}. It happens that the spin-flip Raman cross-section $d\sigma/d\Omega$ in InSb is also unusually large. Yafet [1.63] has shown that

$$d\sigma/d\Omega \cong (e^2 g/2m)(\omega_2/\omega_1)[E_g \hbar\omega_1/(E_g^2 - \hbar^2\omega_1^2)]^2 \qquad (1.16)$$

where m is the electron mass and E_g is the gap energy. For InSb, $E_g = 1900$ cm^{-1}, and then at $\omega_1 \sim 1000$ cm^{-1}, we find $d\sigma/d\Omega \simeq 10^{-23}$ cm^2/sterad. In addition to the large $d\sigma/d\Omega$, spin-flip Raman scattering in InSb also has a very narrow linewidth at low temperatures (~ 0.3 cm^{-1} in an n-type InSb with $n = 10^{16} cm^{-3}$). Consequently, InSb has the largest known Raman gain for all materials. With $\omega_1 = 940$ cm^{-1} (10.6 μm), Patel and Shaw [1.64] found a Raman gain of $G = 1.7 \times 10^{-5} I$ cm^{-1} in an n-type InSb with $n = 3 \times 10^{16} cm^{-3}$, where I is the laser intensity in W/cm^2. One therefore expects that spin-flip SRS in InSb is readily observable. Tunable output from 10.9 to 13.0 μm was first detected by Patel and Shaw [1.24] using a Q-switched CO_2 laser at 10.6 μm. With an input power of 1 KW focused into an area of $10^{-3} cm^2$ in a 5 - mm long InSb crystal ($n \approx 10^{16} cm^{-3}$ at 18°K), they obtained a Stokes output of 10W. The output linewidth was less than 0.03 cm^{-1}. Equation (1.16) shows that if $\hbar\omega_1$ approaches E_g, the Raman cross-section can be resonantly enhanced by several orders of magnitude. Then, the spin-flip SRS can even be operated on a CW basis, as has actually been demonstrated by Brueck and Mooradian [1.65] with a CO laser at 5.3 μm. They found a pump threshold of

less than 50 mW, a power conversion efficiency of larger than 50%, and an output power in excess of 1W. The output linewidth could be less than 1 KHz. [1.66] More recently, using an optically pumped NH_3 laser operating at 12.8 μm, Patel et al. [1.67] has obtained a tuning range of SRS in InSb from 13.9 to 16.8 μm. Spin-flip SRS has also been observed in InAs with an HF laser pump [1.68] and in $Hg_{0.77}Cd_{0.23}Te$ with a CO_2 TEA laser [1.69]. The former has a threshold power of 15W and a conversion efficiency of 20%, and may become an important tunable source in the 3 - 5 μm range. Anti-Stokes radiation and Stokes radiation up to the 4th order have also been observed in spin-flip SRS [1.65,66,70]. They can be used to extend the spectral range of the output. Spin-flip SRS as a tunable infrared source has recently been reviewed by Patel [1.46] and by Colles and Pidgeon [1.47].

Strictly speaking, spin-flip SRS should be treated as a SPS process [1.62] since the spin-flip excitation can also be excited directly by an infrared wave via magnetic-dipole transition, or in other words, the spin-flip excitation is coupled directly with the infrared wave. The coupling

is weak and therefore the corresponding dispersion curve shows very little splitting at the intersection as shown by curve (a) of Fig. 1.2. For this case, the polariton is a highly mixed em and material excitational wave only around the knee of the dispersion curve. If the spin-flip SRS operates with $\vec{k}_3$ (= $\vec{k}_1 - \vec{k}_2$) around the knee, then by the theory of SPS, we should expect to find output radiation at both ω_2 and $\omega_3 (\sim\omega_o)$. Using a CO_2 TEA laser, Shaw [1.71] has recently observed simultaneous output at $\omega_3 \sim \omega_o$ from spin-flip SRS in InSb. It is of course more efficient to generate the far-infrared radiation at $\omega_3 \sim \omega_o$ by pumping the crystal with input beams at both ω_1 and ω_2. This has been done by Nguyen and Bridges [1.28] and is reviewed in Chapter 4.

In many polar crystals, the infrared phonon modes are strongly coupled to the infrared radiation. They form polaritons with dispersion curves that resemble curve (b) in Fig. 1.2. With a fixed pump laser frequency ω_1, the output of SPS at ω_2 and ω_3 can now be tuned by adjusting the relative angle between $\vec{k}_1$ and $\vec{k}_2$ so as to move ω_3 along the polariton dispersion curve to satisfy the phase matching condition $\vec{k}_1 = \vec{k}_2 + \vec{k}_3$. The tuning range depends on the shape of the polariton curve. SPS was first observed by Kurtz and Giordmaine [1.72] and by Gelbwachs et al. [1.73] in $LiNbO_3$ on the 248 cm^{-1} mode. In a resonator, 70% of the laser power can be converted into Stokes at ω_2. Tunable far-infrared output at ω_3 on the same polariton mode in $LiNbO_3$ was later observed by Pantell and coworkers [1.26,74]. It was tuned from 50 μm to 700 μm. The peak power could be as high as 100 W.

Intense anti-Stokes and higher-order Raman radiation can also be generated in SRS. They can be used to extend the output tuning range. We will not discuss the higher-order Raman processes here, but simply refer the readers to the literature (see references in [1.58]).

1.5 Other Methods of Nonlinear Infrared Generation.

Among other methods of nonlinear infrared generation, optically pumped stimulated emission (OPSE) is most attractive. OPSE can be considered as a special case of SRS. We mentioned earlier in Sec. 1.4 that the stimulated Raman gain increases sharply as the pump laser frequency approaches resonance. The resonant enhancement is of course much more significant with narrow but strong resonances. This happens in the case of gas media. In metal vapor, for example, resonant SRS leads to strong tunable infrared output (see Chapter 5). As the pump frequency gets even closer to the resonant line, however, direct absorption of the pump field becomes important and induces a net population change from the ground state $\langle g|$ to the resonant intermediate state $\langle n|$ (see Fig. 1.1). This is known as optical pumping. Following optical pumping, an inverted population can be established between the intermediate state $\langle n|$ and the final state $\langle f|$ so that laser emission may occur. Actually, in this case of a three-level system, both laser emission and SRS operate simultaneously [1.75].

The above picture describes an optically pumped three-level laser system. Such a scheme has been used in atomic and molecular gases to generate a large number of discrete infrared lines. More generally, optical pumping in a multi-level system with subsequent radiative and non-

radiative transfer of population between different levels can establish inverted population for many pairs of states. It can then lead to many more laser lines than the three-level scheme. Thus, for example, in the far-infrared range, several hundreds of OPSE laser lines have already been discovered. Continuous tuning of the laser frequency may become possible with OPSE in high presssure gas systems where the rotational fine structure is smeared out by pressure broadening [1.39]. While OPSE normally generates only discrete infrared laser frequencies, it has the advantages of being highly efficient and operable in a cw mode at the mW level or in a pulsed mode with peak power at the MW level. Infrared generation by OPSE in gases is discussed in great detail in Chapter 6.

Far-infrared radiation of very long wavelength can also be generated by picosecond laser pulses in a crystal [1.76]. This is becuase a 1 - psec pulse has a spectral bandwidth of about 15 cm^{-1} and mixing of the various spectral components of the pulse in the crystal generates far-infrared radiation. Mixing can be achieved either through the second-order nonlinearity in the crystal [1.42,43] or through impurity (or defect) absorption [1.41]. In the former case, the far-infrared output is tunable and can have a linewidth of $\sim$1 cm^{-1} as determined by the phase-matching condition. In the latter case, picosecond excitation of impurities in an acentric polar lattice induces a rapidly varying nonlinear polarization via the pyroelectric effect or/and a change of dipole moment on the impurities. In both cases, with picosecond input pulses, the far-infrared output is often limited to the range between I and 30 cm^{-1}. It is however in the form of a short pulse with a pulsewidth in the picosecond range.

Another novel method of generating coherent tunable infrared radiation is by letting relativistic electrons undergo cyclotron motion in a magnetic field. Granastein et al. [1.45] observed a narrow-band radiation with its peak at the relativistic cyclotron resonance frequency. The peak power was over 1 MW at 7.8 GHz and was greatly enhanced by periodic perturbation of the magnetic field along the field axis. Relativistic electrons in a spatially periodic transverse magnetic field both emits and absorbs radiation via bremsstrahlung and inverse bremsstrahlung respectively. The wavelength for emission is however slightly longer than the wavelength for absorption. This then makes stimulated emission of bremsstrahlung possible [1.77]. Using the relativistic electrons from the superconducting linear accelerator at Stanford, Elias et al. [1.78] recently reported the observation of a stimulated emission gain of 7% per pass at 10.6 μm. The physics of stimulated emission of bremsstrahlung is quite similar to that of stimulated Compton scattering proposed earlier by Pantell et al. [1.79]. However, no experiment on stimulated Compton scattering has yet been reported. Intense microwave emission has also been observed in coherent Cherenkov radiation from a relativistic electron beam interacting with a slow-wave structure [1.80]. The peak power was as high as 500 MW with a 17% conversion efficiency. In principle, the scheme can also be extended to radiation at much shorter wavelengths.

1.6 Summary

We summarize in Table 1.1 the experimental state of art of the various different methods of nonlinear infrared generation. Radiation from a

blackbody at 1000°K is also listed as a comparison. We note that even at this early stage of development, nonlinear infrared generation has already led to tunable infrared sources with both higher peak power and higher average power than the blackbody radiation.

ACKNOWLEDGEMENT

This work is supported by the U. S. Energy Research and Development Administration. The author is indebted to the Miller Institute of the University of California for a research professorship.

REFERENCES

1.1. P. A. Franken, A. E. Hill, C. W. Peters, G. Weinreich, Phys. Rev. Lett. 7, 118 (1961).

1.2. M. Bass, P. A. Franken, A. E. Hill, C. W. Peters, G. Weinreich, Phys. Rev. Lett. 8, 18 (1962).

1.3. A. W. Smith, N. Braslau, IBM Journal Res. 6, 361 (1962).

1.4. M. Bass, P. A. Franken, J. F. Ward, G. Weinreich, Phys. Rev. Lett. 9, 446 (1962).

1.5. J. A. Giordmaine, Phys. Rev. Lett. 8, 19 (1962).

1.6. P. D. Maker, R. W. Terhune, N. Nisenoff, C. M. Savage, Phys. Rev. Lett. 8, 21 (1962).

1.7. J. E. Bjorkholm, Phys. Rev. 142, 126 (1966).

1.8. D. A. Kleinman, A. Ashkin, G. D. Boyd, Phys. Rev. 145, 338 (1966).

1.9. G. D. Boyd, A. Ashkin, J. M. Dziedzic, D. A. Kleinman, Phys. Rev. 137A, 1305 (1965).

1.10. J. A. Giordmaine, R. C. Miller, Phys. Rev. Lett. 14, 973 (1965).

1.11. E. J. Woodbury, W. K. Ng, Proc. IRE 50, 2347 (1962).

1.12. F. Zernike, P. R. Berman, Phys. Rev. Lett. 15, 199 (1965).

1.13. F. Zernike, Bull. Am. Phys. Soc. 12, 687 (1967); Phys. Rev. Lett. 22, 931 (1969).

1.14. T. Yajima, K. Inoue, IEEE J. Quantum Electron. QE-4, 319 (1968); QE-5, 140 (1969); Phys. Lett. 26A, 281 (1968).

1.15. D. W. Faries, K. A. Gehring, P. L. Richards, Y. R. Shen, Phys. Rev. 180, 363 (1969); D. W. Faries, P. L. Richards, Y. R. Shen, K. H. Yang, Phys. Rev. A3, 2148 (1971).

1.16. T. Y. Chang, V. T. Nguyen, C. K. N. Patel, Appl. Phys. Lett. 13, 357 (1968); T. J. Bridges, T. Y. Chang, Phys. Rev. Lett. 22, 811 (1969).

1.17. C. K. N. Patel, V. T. Nguyen, Appl. Phys. Lett. 15, 189 (1969); V. T. Nguyen, C. K. N. Patel, Phys. Rev. Lett 22, 463 (1969).

1.18. V. T. Nguyen, A. R. Strnad, A. M. Jean-Louis, G. Duroffoug, in The Physics of Semimetals and Narrow Gap Semiconductors, D. L. Carter, R. T. Bates, Eds. (Pergamon Press, New York, 1971) p. 231.

1.19. T. J. Bridges, A. R. Strnad, Appl. Phys. Lett. 20, 382 (1972).

1.20. G. D. Boyd, T. J. Bridges, C. K. N. Patel, E. Buchler, Appl. Phys. Lett. 21, 553 (1972).

1.21. See the review articles by R. G. Smith, in "Laser Handbook", edited by F. T. Arecchi, and E. O. Schulz-Dubois, (North Holland, Amsterdam, 1972), p. 837; R. L. Byer, in "Treatise in Quantum Electronics", edited by H. Rabin and C. L. Tang, (Academic, New York, 1975). See also Chapter 3.

1.22. P. O. Sorokin, N. S. Shiren, J. R. Lankard, E. C. Hammond, T. G. Kazyaka, Appl. Phys. Lett. 10, 44 (1967).

1.23. M. Rokni, S. Yatsiv, Phys. Lett. A24, 277(1967); IEEE J. Quant. Electron. QE3, 329 (1967).

1.24. C. K. N. Patel, E. D. Shaw, Phys. Rev. Lett. 24, 451 (1970).

1.25. T. Y. Chang, T. J. Bridges, Optics Comm. 1, 423 (1970).

1.26. J. M. Yarborough, S. S. Sussman, H. E. Puthoff, R. H. Pantell, B. C. Johnson, Appl. Phys. Lett. 15, 102 (1969).

1.27. C. F. Dewey, L. O. Hocker, Appl. Phys. Lett. 18, 58 (1971).

1.28. V. T. Nyguyen, T. J. Bridges, Phys. Rev. Lett. 29, 359 (1972).

1.29. N. Matsumoto, T. Yajima, Jap. J. Appl. Phys. 12, 90 (1973).

1.30. K. H. Yang, J. R. Morris, P. L. Richards, Y. R. Shen, Appl. Phys. Lett. 23, 669 (1973).

1.31. P. P. Sorokin, J. J. Wynne, J. R. Lankard, Appl. Phys. Lett. 22, 342 (1973).

1.32. R. L. Aggarwal, B. Lax, G. Favrot, Appl. Phys. Lett. 22, 329 (1973); B. Lax, R. L. Aggarwal, G. Favrot, Appl. Phys. Lett. 23, 679 (1973).

1.33. R. L. Aggarwal, B. Lax, H. R. Fetterman, P. E. Tannenwald B. J. Clifton, J. Appl. Phys. 45, 3972 (1974); N. Lee, R. L. Aggarwal, B. Lax, Optics Comm. 11, 339 (1974).

1.34. J. A. Armstrong, N. Bloembergen, J. Ducuing, P. S. Pershan, Phys. Rev. 127, 198 (1962).

1.35. T. J. Bridges, V. T. Nguyen, E. G. Burkhardt, C. K. N. Patel, Appl. Phys. Lett. 27, 600 (1975).

1.36. D. E. Thompson, P. D. Coleman, IEEE Trans. MTT-22, 995 (1974).

1.37. J. L. Carlsten, T. J. McIlrath, J. Phys. B6, L80 (1973); J. L. Carlsten, P. C. Dunn, Optics. Comm. 14, 8 (1975); D. Cotter, D. C. Hanna, P. A. Karkkainen, R. Wyatt, Optics Comm. 15, 143 (1975); D. Cotter, D. C. Hanna, R. Wyatt, Optics. Comm. 16, 256 (1976).

1.38. W. Schmidt, W. Appt, Naturforsch, 27a, 1373 (1972). Abstracts of VIII International Quantum Electronic Conference (San Francisco,

1974), Post-deadline paper R 6; R. Frey, F. Pradere, Optics Comm. 12, 98 (1974).

1.39. T. Y. Chang, O. R. Wood, Appl. Phys. Lett. 23, 370 (1973); 24, 182 (1974).

1.40. R. L. Byer, R. L. Herbst, R. N. Fleming, in Proceedings of the Second International Conference on Laser Spectroscopy, edited by S. Haroche, J. C. Pebay-Peyroula, T. W. Hansch, and S. E. Harris (Springer Verlag, 1975) p. 207.

1.41. D. H. Auston, A. M. Glass, A. A. Ballman, Phys. Rev. Lett 28, 897 (1972); D. H. Auston, A. M. Glass, Appl. Phys. Lett. 20, 398 (1972); A. M. Glass, D. H. Auston, Optics Comm. 5, 45 (1972); D. H. Auston, A. M. Glass, P. LeFur, Appl. Phys. Lett. 23, 47 (1973).

1.42. K. H. Yang, P. L. Richards, Y. R. Shen, Appl. Phys. Lett. 19, 385 (1971).

1.43. T. Yajima, N. Takeuchi, Jap. J. Appl. Phys. 10, 907 (1971).

1.44 R. L. Byer, R. L. Herbst, in Chapter 3 of this book.

1.45. V. L. Granatstein, M. Herndon, R. K. Parker, S. P. Schlesinger, IEEE J. Quantum Electron. 10, 651 (1974); IEEE Trans. Microwave Theory Tecn. 22, 1000 (1974).

1.46. C. K. N. Patel, in "Fundamental and Applied Laser Physics", edited by M. S. Feld, A. Javan, and N. A. Kurnit, (J. Wiley, New York, 1972) p. 689; in "Laser Spectroscopy", edited by R. G. Brewer and A. Mooradian, (Plenum Press, New York, 1974), p. 471.

1.47. M. J. Colles; C. R. Pidgeon, Reports on Progress in Physics 38, 387 (1975).

1.48. Y. R. Shen, Progress in Quantum Electronics 4, 207 (1976).

1.49. See, for example, N. Bloembergen, "Nonlinear Optics" (Benjamin, New York, 1965).

1.50. J. R. Morris, Y. R. Shen, (to be published).

1.51. D. W. Faries, Ph.D. Thesis, Univ. of California at Berkeley, (1970).

1.52. C. C. Wang, G. W. Racette, Appl. Phys. Lett. 6, 169 (1965).

1.53. R. L. Herbst, R. L. Byer, Appl. Phys. Lett. 21, 189 (1972).

1.54. D. C. Hanna, B. Luther-Davis, R. C. Smith, Appl. Phys. Lett. 22, 440 (1974).

1.55. A. Laubereau, L. Greiter, W. Kaiser, Appl. Phys. Lett. 25, 87 (1974); T. Kushida, Y. Tanaka, M. Ojima, Y. Nakazaki, Japan. J. Applied Phys. 14, 1097 (1975).

1.56. N. Bloembergen, Am. J. Phys. 35, 989 (1967).

1.57. W. Kaiser, M. Maier, in "Laser Handbook" edited by F. T. Arecchi and E. O. Schulz-Dubois (North-Holland, Amsterdam, 1972) p. 1077.

1.58. Y. R. Shen, in "Raman Scattering in Solids", edited by M. Cardona (Springer, Berlin, 1975) p. 275.

1.59. Y. R. Shen, N. Bloembergen, Phys. Rev. 137, A1786 (1965).

1.60. Y. R. Shen, Phys. Rev. 138, A1741 (1965).

1.61. K. Huang, Nature 167, 779 (1951); Proc. Roy. Soc. (London) A208, 352 (1951); J. J. Hopfield, Phys. Rev. 112, 1555 (1958).

1.62. Y. R. Shen, Appl. Phys. Lett. 26, 516 (1973).

1.63. Y. Yafet, Phys. Rev. 152, 858 (1966).

1.64. C. K. N. Patel, E. D. Shaw, Phys. Rev. B3, 1279 (1971).

1.65. S. J. Brueck, A. Mooradian, Appl. Phys. Lett. 18, 229 (1971).

1.66. C. K. N. Patel. Phys. Rev. Lett. 28, 649 (1972).

1.67. C. K. N. Patel, T. Y. Chang, V. T. Nguyen, App. Phys. Lett. 28, 603 (1976).

1.68. R. S. Eng, A. Mooradian, H. R. Fetterman, Appl. Phys. Lett. 25, 453 (1974).

1.69. J. R. Sattler, B. A. Weber, J. Nemarich, Appl. Phys. Lett. 25, 451 (1974).

1.70. A. Mooradian, S. R. J. Brueck, F. A. Blum, Appl. Phys. Lett. 17, 481 (1970); E. D. Shaw, C. K. N. Patel, Appl. Phys. Lett. 18, 215 (1971); C. S. DeSilets, C. K. N. Patel, Appl. Phys. Lett. 22, 543 (1973).

1.71. E. Shaw, Bull. Am. Phys. Soc. 21, 224 (1976).

1.72. S. K. Kurtz, J. A. Giordmaine, Phys. Rev. Lett. 22, 192 (1969).

1.73. J. Gelbwachs, R. H. Pantell, H. E. Puthoff, J. M. Yarborough, Appl. Phys. Lett. 14, 258 (1969).

1.74. M. A. Piestrup, R. N. Fleming, R. H. Pantell, Appl. Phys. Lett. 26, 418 (1975).

1.75. A. Javan, Phys. Rev. 107, 1579 (1957); K. Shimoda, T. Shimizu, Progress in Quantum Electronics 2,61 (1972); Y. R. Shen, Phys. Rev. B9, 622 (1973).

1.76. J. R. Morris, Y. R. Shen, Optics Comm. 3, 81 (1971).

1.77. M. J. Madey, J. Appl. Phys. 42, 1906 (1971); M. J. Madey, H. A. Schwettman, W. M. Fairbank, IEEE Trans. Nuc.Sci. 20, 980 (1973).

1.78. L. R. Elias, W. M. Fairbank, J. M. J. Madey, H. A. Schwettman, T. I. Smith, Phys. Rev. Lett. 36. 717 (1976).

1.79. R. H. Pantell, G. Soncini, H. E. Puthoff, IEEE J. Quantum Electron. QE-4, 905 (1968).

1.80. Y. Carmel, J. Ivers, R. E. Kribel , J. Nation, Phys. Rev. Lett. 33, 1278 (1974).

FIGURE CAPTIONS

Fig. 1.1. Schematic drawing showing the Stokes ($\omega_1 > \omega_2$) and anti-Stokes ($\omega_1 < \omega_2$) Raman transition between the ground state $|g\rangle$ and the excited state $|f\rangle$.

Fig. 1.2. Polariton dispersion curves. (a) Weak coupling and (b) strong coupling between electromagnetic and material excitational waves.

TABLE CAPTION

Table 1.1. Present status of various methods of nonlinear infrared generation. The output of a blackbody radiation is shown for comparison.

TABLE I

Technique	Mode of Operation	Tuning Range (cm^{-1})	Average or Peak Power Obtained	Spectral Width (cm^{-1})	Pumped Lasers
Difference-frequency mixing in crystals	Pulsed	1 - 200	0.1 W	< 0.1	Ruby/Dye or
	Pulsed	600 - 10,000	300 W	< 0.1	2 Dye lasers
	Pulsed	420 - 6,000	10 W	< 0.1	2 Parametric Oscillators
	Pulsed	5 - 140 in 3200 steps	10 W	< 0.1	2 CO_2 lasers
	CW	5 - 140 in 3200 steps	0.1 μW	< $3x10^{-3}$	2 CO_2 lasers
	CW	2,380 - 4,550	1 μW	$5x10^{-4}$	Ar^+/Dye
Mixing via spin-flip transition	Pulsed	possibly 10 - 300	2 μW	< 0.1	CO_2/Spin-Flip
Mixing in metal vapor	Pulsed	400 - 5,000	0.1 W	< 0.1	2 Dye lasers
Parametric Oscillator	Pulsed	900 - > 10,000	~1 MW	0.03	Nd: YAG
Stimulated Raman scattering in vapor	Pulsed	670 - 10,000	60 MW	0.2	Dye
Stimulated spin-flip Raman scattering	Pulsed	590 -1100 1540 - 2000	200 W	0.03	CO_2 or NH_3
	CW	1540 - 2000	1 W	$3x10^{-6}$	CO
Stimulated polariton scattering	Pulsed	14 - 200	100 W	< 1	Ruby
1-cm^2 Blackbody Radiation at 1000°K with a 10 mrad. angular spread	CW		0.06 μW/cm^{-1} at 1000 cm^{-1} $1.2x10^{-3}$ μW/cm^{-1} at 100 cm^{-1} $1.3x10^{-5}$ μW/cm^{-1} at 10 cm^{-1}		

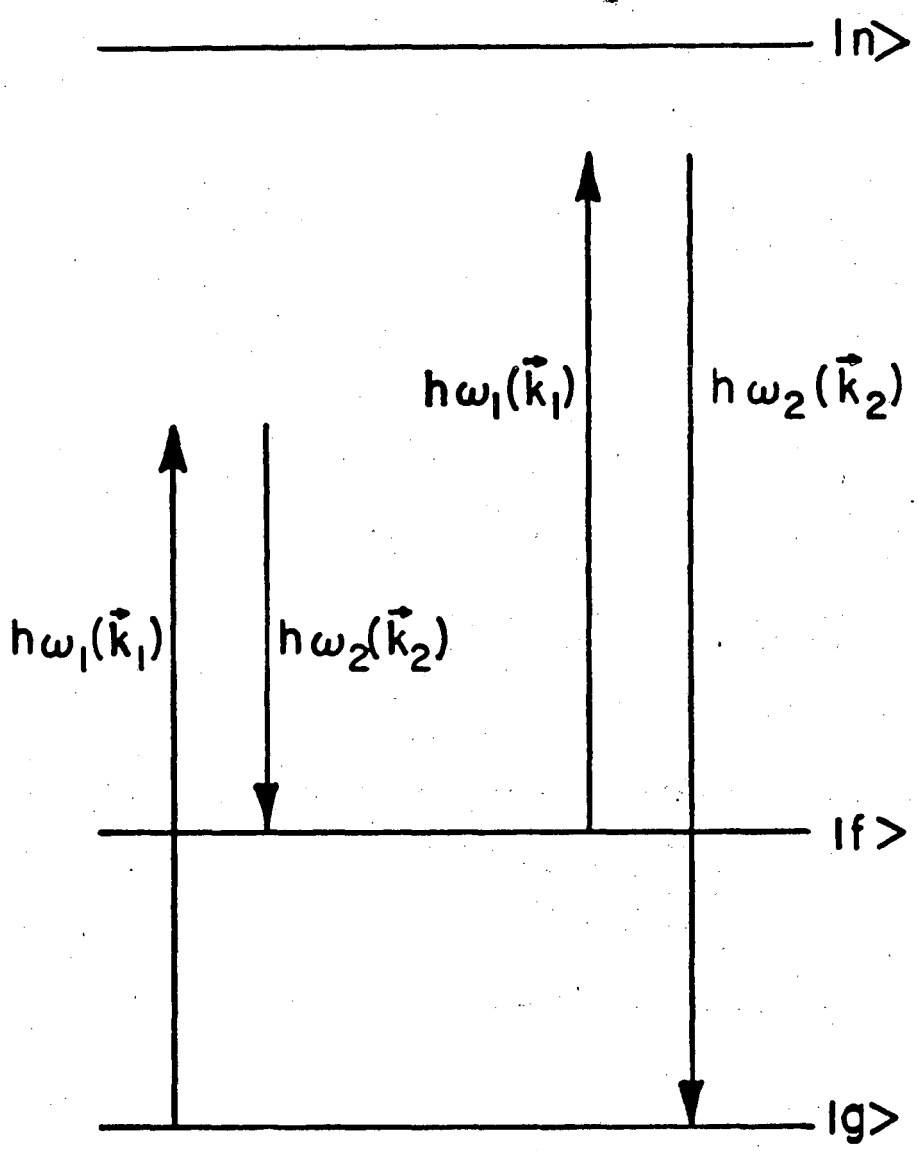

Fig. 1.1

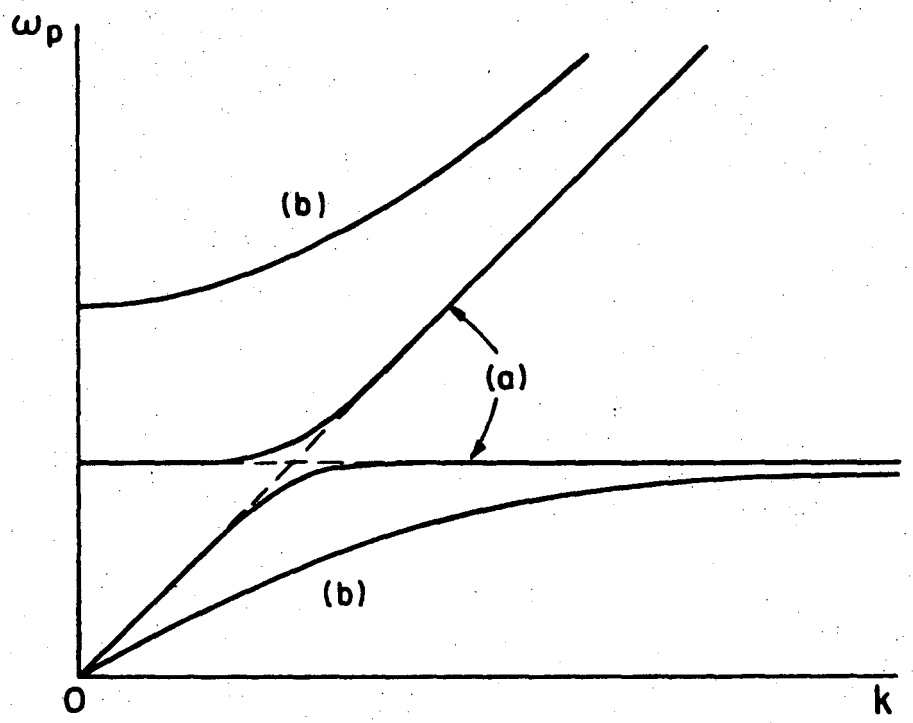

XBL755-6342

Fig. 1.2

TECHNICAL INFORMATION DIVISION
LAWRENCE BERKELEY LABORATORY
UNIVERSITY OF CALIFORNIA
BERKELEY, CALIFORNIA 94720